Dimuon radiation at relativistic energies available at the CERN Super Proton Synchrotron within a (3 + 1)D hydrodynamic + cascade model

E. Santini,[1,2] J. Steinheimer,[1,2] M. Bleicher,[1,2] and S. Schramm[2]

[1]*Institut für Theoretische Physik, Goethe-Universität, Max-von-Laue-Str. 1, D-60438 Frankfurt am Main, Germany*

[2]*Frankfurt Institute for Advanced Studies (FIAS), Ruth-Moufang-Str. 1, D-60438 Frankfurt am Main, Germany*

(Received 13 January 2011; published 15 July 2011)

We analyze dilepton emission from hot and dense matter using a hybrid approach based on the ultrarelativistic quantum molecular dynamics (UrQMD) transport model with an intermediate hydrodynamic stage for the description of heavy-ion collisions at relativistic energies. During the hydrodynamic stage, the production of lepton pairs is described by radiation rates for a strongly interacting medium in thermal equilibrium. In the low-mass region, hadronic thermal emission is evaluated by assuming vector meson dominance including in-medium modifications of the ρ meson spectral function through scattering from nucleons and pions in the heat bath. In the intermediate-mass region, the hadronic rate is essentially determined by multipion annihilation processes. Emission from quark-antiquark annihilation in the quark gluon plasma (QGP) is taken into account as well. When the system is sufficiently dilute, the hydrodynamic description breaks down and a transition to a final cascade stage is performed. In this stage dimuon emission is evaluated as commonly done in transport models. By focusing on the enhancement with respect to the contribution from long-lived hadron decays after freezeout observed at the SPS in the low-mass region of the dilepton spectra, the relative importance of the different thermal contributions and of the two dynamical stages is investigated. We find that three separated regions can be identified in the invariant mass spectra. Whereas the very low and the intermediate-mass regions mostly receive contribution from the thermal dilepton emission, the region around the vector meson peak is dominated by the cascade emission. Above the ρ-peak region the spectrum is driven by QGP radiation. Analysis of the dimuon transverse mass spectra reveals that the thermal hadronic emission shows an evident mass ordering not present in the emission from the QGP. A comparison of our calculation to recent acceptance-corrected NA60 data on invariant as well as transverse mass spectra is performed.

DOI: 10.1103/PhysRevC.84.014901 PACS number(s): 24.10.Lx, 25.75.Dw, 25.75.Cj

I. INTRODUCTION

Dileptons represent a penetrating probe of the hot and dense nuclear matter created in heavy-ion collisions since, once produced, they essentially do not interact with the surrounding hadronic matter. The analysis of the electromagnetic response of the dense and hot medium is tightly connected to the investigation of the in-medium modification of the vector meson properties. Vector mesons are ideally suited for this exploration, because they can directly decay into a lepton-antilepton pair. One therefore aims to infer information on the modifications induced by the medium on specific properties of the vector meson, such as its mass and/or its width, from the invariant mass dilepton spectra.

The NA60 experiment at CERN SPS has recently measured the invariant mass spectra of low-mass dimuons [1–4]. As in previous ultrarelativistic heavy ion collision experiments [5,6], at low invariant masses an enhancement of dilepton pairs in heavy systems as compared to the expected contribution from decays of long-lived hadrons (mostly η, η', ω, and ϕ mesons), commonly referred to as "hadron cocktail," was observed. The high data quality of NA60 allowed the subtraction of the cocktail of the decay sources from the total data and the isolation of the excess pairs. One of the first results was strong evidence for the presence of broadening of the spectral function of the ρ meson [1].

From the first communication by the NA60 Collaboration [1], the remaining excess of pairs (often referred to as "the excess") has been the object of various theoretical investigations. Phenomenological models have been refined and extended to include the various sources of dilepton production, and an almost comprehensive [7–12] interpretation of the invariant mass spectra of the excess has been reached. Calculations performed by convolution of dilepton production rates, using the assumption of local equilibrium, over the space-time evolution of the medium modeled according to simple expanding fireball approaches have been quite successful in explaining the dilepton excess observed at SPS [7,9,11,12].

This use of basic approaches for the modeling of the heavy-ion collision dynamics focused the investigations on the various scenarios for the in-medium modification of the vector meson properties, and evidence for a broadening of the ρ meson spectral function was inferred from the comparison to the measurements. However, in these models the time development of the reaction is not described by fully dynamical simulations but rather parametrized in terms of the estimated time which the system spends in the various phases. Though such parametrizations can be properly tuned and constrained, a more complete treatment of the heavy-ion dynamics in terms of transport and/or fully (3 + 1)-dimensional hydrodynamical models should be in order, since a good knowledge of the temperature, baryon-density, and flow evolution is necessary to convert dilepton rates into space-time integrated spectra.

Earlier, a (2 + 1)-dimensional hydrodynamical description of dilepton production has been performed by Huoviven

et al. [13–15] and compared to data from the first generation of dilepton experiments performed in the 1990s. However, already at that time [15] it was shown that the evolution can have a strong impact on the dilepton yields. To our knowledge, the model was never applied to the high-resolution NA60 data. Application of hydrodynamics to analyze the dimuon excess observed by NA60 was performed by Dusling *et al.* [8,10] using a boost-invariant $(1+1)$-dimensional hydrodynamical model. If on one side this represents a step further toward the inclusion of more realistic dynamics, on the other side boost-invariant hydrodynamics is expected to be an approximation more valid at RHIC energies than at SPS. In Ref. [16], e.g., it was shown that the photon spectra measured by the WA98 Collaboration at the CERN SPS [17] could be accounted for in a boost-invariant scenario only by choosing a short initial time ($\tau_0 = 0.3$ fm), which is not in accordance with the expected longitudinal geometry. In this respect, it is surely desirable to relax this approximation and use a full $(3+1)$ hydrodynamic expansion.

Moreover, the contribution to the excess of nonthermal dilepton radiation from short-lived mesons has only very recently received proper attention by the theoretical groups mostly active in the field of thermal dileptons. For example, in Ref. [8] the contribution from freezeout ρ mesons was neglected and added only in a later work [10], whereas in Ref. [12] an explicit treatment of ρ decays at thermal freezeout together with the additional inclusion of a nonthermal component of primordially produced ρ mesons which escape the fireball was required in order to account for some discrepancy with thermal emission revealed by analysis of measured transverse pair momenta (p_T) spectra at $p_T > 1$ GeV.

In this paper, we want to directly address these aspects, presenting a consistent calculation of the dilepton production at SPS energy within a model which attempts to take into account both the complexity of the dilepton rate in a hot dense medium as well as the complexity of the pre-, post-, and equilibrium heavy-ion dynamics. The latter is modeled with an integrated Boltzmann+hydrodynamics hybrid approach based on the ultrarelativistic quantum molecular dynamics (UrQMD) transport model with an intermediate $(3+1)$-dimensional ideal hydrodynamic stage. For earlier investigations within hybrid approaches see, e.g., [18–20]. The hybrid approach used here has been successfully applied to many bulk observables and photon spectra [21] at SPS energies. For the present investigation, during the local equilibrium phase, the radiation rate of the strongly interacting medium is standardly modeled using the vector meson dominance model and related to the spectral properties of the light vector mesons, with the ρ meson having the dominant role. In-medium modifications of the ρ-meson spectral function due to scattering from hadrons in the heat bath are properly included in the model. Two additional sources of thermal radiation, namely emission from multipion annihilation processes and from a thermalized partonic phase, are included as well.

The paper is organized as follows. In Sec. II, we briefly discuss the hybrid model and present the emission rates of the various sources taken into account. In Sec. III we present results for the dilepton excess invariant mass spectra and transverse mass spectra. A comparison to the NA60 data is performed. Section IV is dedicated to a discussion of the various components that enter the contribution of the cascade stage of the hybrid approach. Finally, a summary and conclusions are given in Sec. V.

II. THE MODEL

A. The hybrid approach

To simulate the dynamics of the In + In collisions we employ a transport approach with an embedded three-dimensional ideal relativistic one-fluid evolution for the hot and dense stage of the reaction based on the UrQMD model. The present hybrid approach has been extensively described in Ref. [22] and first applications to electromagnetic probes have been recently performed [21,23–26]. Here, we limit ourselves to briefly describe its main features and refer the reader to Ref. [22] for details.

UrQMD [27–29] is a hadronic transport approach which simulates multiple interactions of ingoing and newly produced particles, the excitation and fragmentation of color strings, and the formation and decay of hadronic resonances. The coupling between the UrQMD initial state and the hydrodynamical evolution proceeds when the two Lorentz-contracted nuclei have passed through each other. Here, the spectators continue to propagate in the cascade and all other hadrons are mapped to the hydrodynamic grid. Event-by-event fluctuations are directly taken into account via initial conditions generated by the primary collisions and string fragmentations in the microscopic UrQMD model. This leads to nontrivial velocity and energy density distributions for the hydrodynamical initial conditions in each single event [30,31]. Subsequently, a full $(3+1)$-dimensional ideal hydrodynamic evolution is performed using the SHASTA algorithm [32,33]. The hydrodynamic evolution is gradually merged into the hadronic cascade: to mimic an iso-eigentime hypersurface, full transverse slices, of thickness $\Delta z = 0.2$ fm, are transformed to particles whenever in all cells of each individual slice the energy density drops below five times the ground-state energy density. The employment of such a gradual transition allows one to obtain a rapidity-independent transition temperature without artificial time dilatation effects [34,35] and has been explored in detail in various recent works [34,36–38] devoted to SPS conditions. When merging, the hydrodynamic fields are transformed to particle degrees of freedom via the Cooper-Frye equation [39] on the hypersurface σ_μ,

$$p_0 \frac{dN}{d^3p} = \int_\sigma f(x,p) p^\mu d\sigma_\mu, \tag{1}$$

where $f(x,p)$ are the boosted Fermi or Bose distributions corresponding to the respective particle species. For the present analysis, the latter was modified in order to account for the spectral shape of the ρ meson via the substitution

$$\frac{d^3p}{p_0} \to \frac{d^3p}{p_0} dM^2 \delta^+\left(M^2 - m_\rho^2\right) \to d^4p 2A_\rho(M), \tag{2}$$

with $A_\rho(M) = -\frac{1}{\pi} Im D_\rho(M)$ being the ρ meson spectral function and $D_\rho(M)$ being the ρ meson propagator in vacuum.

The created particles then proceed in their evolution in the hadronic cascade where rescatterings and final decays occur until all interactions cease and the system decouples.

An input for the hydrodynamical calculation is the equation of state (EoS). In this work we employ an equation of state in line with lattice data that follows from coupling the Polyakov loop to a chiral hadronic flavor SU(3) model [40]. The hadronic part is an extension of a nonlinear representation of a sigma-omega model including the lowest-lying multiplets of baryons and mesons. (For the derivation and a detailed discussion of the hadronic part of the model Lagrangian see [41–43].) In a spirit similar to the Nambu-Jona-Lasinio model with the Polyakov loop (PNJL model) [44] it includes the Polyakov loop as an effective field and adds quark degrees of freedom. In this configuration the EoS describes chiral restoration as well as the deconfinement phase transition, while it contains the correct asymptotic degrees of freedom (quarks ↔ hadrons). For details, we refer the reader to Ref. [40].

B. Thermal contributions to the dimuon excess: emission rates

During the locally equilibrated hydrodynamical stage, dimuon emission is calculated locally in space-time, i.e., for each cell of the $(3+1)$ hydrodynamical grid, according to the expression for the thermal equilibrium rate of dilepton emission per four-volume and four-momentum from a bath at temperature T and baryon chemical potential μ_B. The total dimuon yield is then obtained by integrating the emission rate over all fluid cells and all time steps of the $(3+1)$ grid that are spanned by the system during the hydrodynamical evolution until the transition criterion is reached.

In the low invariant mass region of the dilepton spectrum ($M < 1$ GeV) the largest contribution to the dilepton excess is due to the $\rho^0 \to l^+l^-$ emission. As pointed out in various works (see, e.g., [11,12,45,46]), when invoking the vector meson dominance model, the thermal rate can be related to the spectral properties of the vector mesons. Retaining only the contribution of the ρ meson (which is the largest), one arrives at the following expression [46]:

$$\frac{d^8N_{\rho\to ll}}{d^4x d^4q} = -\frac{\alpha^2 m_\rho^4}{\pi^3 g_\rho^2}\frac{L(M^2)}{M^2} f_B(q_0;T)\mathrm{Im}D_\rho(M,q;T,\mu_B), \tag{3}$$

where $\alpha = e^2/(4\pi) = 1/137$ denotes the fine-structure constant, $M^2 = q_0^2 - q^2$ is the dilepton invariant mass squared with energy q_0 and three-momentum q, $f_B(q_0;T)$ is the thermal Bose distribution function, $L(M^2)$ is the lepton phase space factor,

$$L(M^2) = \left(1+\frac{2m_l^2}{M^2}\right)\sqrt{1-\frac{4m_l^2}{M^2}}, \tag{4}$$

which quickly approaches one above threshold, and $\mathrm{Im}D_\rho(M,q;T,\mu_B)$ is the imaginary part of the in-medium ρ meson propagator

$$D_\rho(M,q;T,\mu_B) = \frac{1}{M^2 - m_\rho^2 - \Sigma_\rho(M,q;T,\mu_B)}. \tag{5}$$

Here, m_ρ denotes the pole mass and $\Sigma_\rho(M,q;T,\mu_B)$ the in-medium self-energy. In this application, the self-energy contributions taken into account are the following:

$$\Sigma_\rho(M,q;T,\mu_B) = \Sigma^0(M) + \Sigma^{\rho\pi}(q;T) + \Sigma^{\rho N}(q;T,\mu_B), \tag{6}$$

where $\Sigma^0(M)$ is the vacuum self-energy and $\Sigma^{\rho\pi}(q;T)$ and $\Sigma^{\rho N}(q;T,\mu_B)$ denote the contribution to the self-energy due to the direct interactions of the ρ with, respectively, pions and nucleons of the surrounding heat bath. The latter have been calculated according to Ref. [47], where they were evaluated in terms of empirical scattering amplitudes from resonance dominance at low energies and Regge-type behavior at high energy. In principle, the matter part of the self-energy should depend on M and q (or on q^0 and q) separately. Here, it depends only on q because in Ref. [47] the scattering amplitudes were evaluated on the mass shell of the ρ meson.

Our analysis of the invariant mass dilepton spectrum is restricted to $M < 1.5$ GeV. In the mass region $1 < M < 1.5$ GeV the sources expected to give a major contribution to the dilepton excess are the multipion emission and the $q\bar{q}$ annihilation in the quark gluon plasma (QGP). A third background source usually present in the intermediate-mass region, the correlated decays of D and $\bar{D}$ mesons, could be disentangled from the prompt excess via vertex reconstruction [48] and has been recently subtracted from the NA60 data on the excess [3].

The four-pion contribution is the major manifestation of the multipion emission for the region of our interest, $1 < M < 1.5$ GeV, and will be included in this analysis. The six-pion contribution and other multihadron interactions are not included since they start to play a non-negligible role only for masses $M \gtrsim 1.8$ GeV. Following Huang's observation [49] that lepton pair production can be determined from the electromagnetic spectral function extracted in e^+e^- annihilation, we estimate the contribution of the $4\pi \to l^+l^-$ process to the dilepton rate as

$$\frac{d^8N_{4\pi\to ll}}{d^4x d^4q} = \frac{4\alpha^2}{(2\pi)^2} e^{-q_0/T}\frac{M^2}{16\pi^3\alpha^2}\sigma(e^+e^-\to 4\pi). \tag{7}$$

The above expression neglects the soft-pion final-state-interaction corrections that induce the mixing between the axial-vector and vector currents. We postpone the investigation of the effects caused by the parity mixing phenomenon to a future work and, here, restrict ourselves to mention that the mixing is expected to enhance the rate in the invariant mass region $1 < M < 1.3$ GeV [49]. Calculations that include the axial vector-vector mixing can be found in Refs. [7,12].

For the specific purposes of this work, it is sufficient to use an empirical approach and estimate the four-pion contribution to the dilepton spectra directly from the measured cross sections, without attempting any phenomenological modeling of the underlying processes. We consider the multipion reactions $e^+e^- \to \pi^+\pi^-\pi^+\pi^-$ and $e^+e^- \to \pi^+\pi^-\pi^0\pi^0$. As a side remark, we mention that models based on effective Lagrangians suggest that these reactions are dominated by processes involving the two-body intermediate state $a_1(1260)\pi$ [50,51]. For the cross section of the $e^+e^- \to \pi^+\pi^-\pi^+\pi^-$

process we use the recent precise BaBar data [52] which cover a large range of center-of-mass energies. The measured cross section is in good agreement with the high-precision data taken at VEPP-2M by SND [53] and CMD-2 [54,55] in the energy range 0.7–1.4 GeV, as well as with data obtained at DCI by DM2 [56] in the 1.4–2.0 GeV range. In a similar spirit, for the cross section of the process $e^+e^- \to \pi^+\pi^-\pi^0\pi^0$, we take preliminary results of the BaBar Collaboration [57], which agree with SND [53] measurements in the energy range below 1.4 GeV.

Finally, the $q\bar{q} \to \gamma^* \to l^+l^-$ emission is evaluated according to [58] as

$$\frac{dN_{q\bar{q}\to ll}}{d^4x d^4q} = \frac{\alpha^2}{4\pi^4}\frac{T}{q} f_B(q_0;T)\sum_q e_q^2 \ln\frac{(x_- + \exp[-(q_0+\mu_q)/T])(x_+ + \exp[-\mu_q/T])}{(x_+ + \exp[-(q_0+\mu_q)/T])(x_- + \exp[-\mu_q/T])}, \tag{8}$$

with $x_\pm = \exp[-(q_0 \pm q)/2T]$ and μ_q the quark chemical potential.

Equations (3), (7) and (8) are valid in the rest frame of the fluid. For a moving fluid the Bose-Boltzmann distribution function must be substituted with the Jüttner function. The modulus of the three-momentum can be expressed as a function of the Lorentz-invariant variables M and $q_\mu u^\mu$ (where u^μ denotes the four-velocity of the fluid cell) as $\sqrt{(q_\mu u^\mu)^2 - M^2}$, so that, e.g., the in-medium ρ meson propagator in Eq. (3) can be expressed as $D_\rho(M, \sqrt{(q_\mu u^\mu)^2 - M^2}; T, \mu_B)$. In brief, the substitution $(q_0, q) \to (q_\mu u^\mu, \sqrt{(q_\mu u^\mu)^2 - M^2})$ must be performed on the right-hand side of Eqs. (3), (7), and (8).

The χ-EoS used in this analysis includes an extended crossover between the hadronic and the QGP phase during which the two states of matter coexist. The fraction of QGP in the medium is estimated as the ratio between the energy density stored in quarks and gluons degrees of freedom and the total energy density. We denote this ratio as $\lambda = \lambda(T, \mu_q)$. Typical values of λ as a function of temperature T and quark chemical potential μ_q are shown in Fig. 1. For a given configuration of (T, μ_q) of a fluid cell, we weight the hadronic radiation rate with the function $(1 - \lambda)$ and the $q\bar{q}$ annihilation rate with the function λ. Thus, each cell contributes to the total dimuon emission rate according to

$$\frac{d^8N_{ll}}{d^4x d^4q} = [1-\lambda(T,\mu_q)]\left(\frac{d^8N_{4\pi\to ll}}{d^4x d^4q} + \frac{d^8N_{\rho\to ll}}{d^4x d^4q}\right) + \lambda(T,\mu_q)\frac{dN_{q\bar{q}\to ll}}{d^4x d^4q}. \tag{9}$$

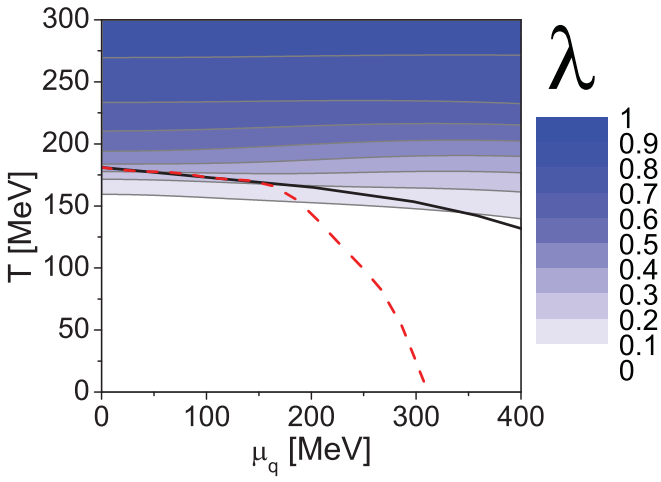

FIG. 1. (Color online) Fraction of QGP for various values of temperature and quark chemical potential. The dashed line indicates where the change of the chiral condensate with respect to T and μ_q has a maximum while the solid line shows the same for the change of the Polyakov loop. See Ref. [40] for details.

C. Cascade contribution to the dimuon excess

In the evolution stages that precede or follow the hydrodynamic phase, dimuon emission from the ρ meson is calculated as in Refs. [23,59] by employing the time integration method (often also called the "shining method") that has since long been applied in the transport description of dilepton emission (see, e.g., [59–62]). Note that in the pre- and post-hydrodynamical stages the particles are the explicit degrees of freedom and all their interactions are treated explicitly within the cascade transport approach. This allows one to dynamically account for final-state interactions during the late stage of the reaction and to follow the continuous decoupling of the different particles, since sequential freezeout of different particle species occurs depending on the microscopic reaction rates. For such a minutely detailed microscopic description of the evolution of the system, however, there is a price to pay, namely that the cascade model solely treats collisions and decays on the basis of vacuum cross sections and decay rates. Thus, eventual residual in-medium modifications of the ρ meson spectral function in this last stage will be neglected when adopting the present model. In fact, the consistent treatment of broad spectral structures within the transport approach is not trivial. Many works have been dedicated to this topic (e.g., Refs. [63–69]); for an overview we refer the reader to the recent critical review by Knoll [70].

Emission from the stage preceding the hydrodynamical evolution is typically small, since the geometrical criteria adopted to start the hydrodynamical evolution corresponds to a starting time $t_{\text{start}} \approx 1.16$ fm at top SPS energy. Emission from the stage that follows the hydrodynamical evolution receives two main contributions: when merging the hydrodynamical stage to the UrQMD model to perform the final cascade, the hydrodynamic fields are mapped to hadrons according to the Cooper-Frye equation. At this point a certain number of primary ρ^0s are

created and enter the cascade. If soon after the transition the system is decoupled with respect to processes involving ρ mesons, during the cascade these primary ρ^0 mesons simply decay, no further ρ^0s are generated, and the corresponding dilepton yield is determined by the abundance of ρ^0 mesons created at the transition times the dilepton branching. If the system is not decoupled with respect to processes involving ρ mesons, as presumably in reality and in the present model (as we will show), ρ meson (re)generation and absorption will occur through processes such as $\pi\pi$ annihilation and resonance decays. These processes will delay the decoupling, increasing the emission time, and, consequently, the dilepton yield.

III. COMPARISON TO NA60 DATA

A. Centrality selection

The NA60 Collaboration has recently presented data fully corrected for geometrical acceptance and pair efficiencies of the NA60 detector [3]. The acceptance-corrected data correspond to nearly minimum bias collisions, selecting events with a charged particle density $dN_{ch}/d\eta > 30$. In order to select the appropriate impact parameter range in our simulations, we first simulate minimum bias collisions and determine the charged particle density as a function of the impact parameter. The result is shown in Fig. 2. We find that $dN_{ch}/d\eta > 30$ corresponds to $b < 9$ fm. With this selection, we obtain an average charged particle density $\langle dN_{ch}/d\eta\rangle = 115$, a value that deviates from the measured one $\langle dN_{ch}/d\eta\rangle = 120$ only by 4%.

B. Invariant mass spectra

In Fig. 3 we show results for the invariant mass spectra of the excess dimuons in various slices in the transverse momentum

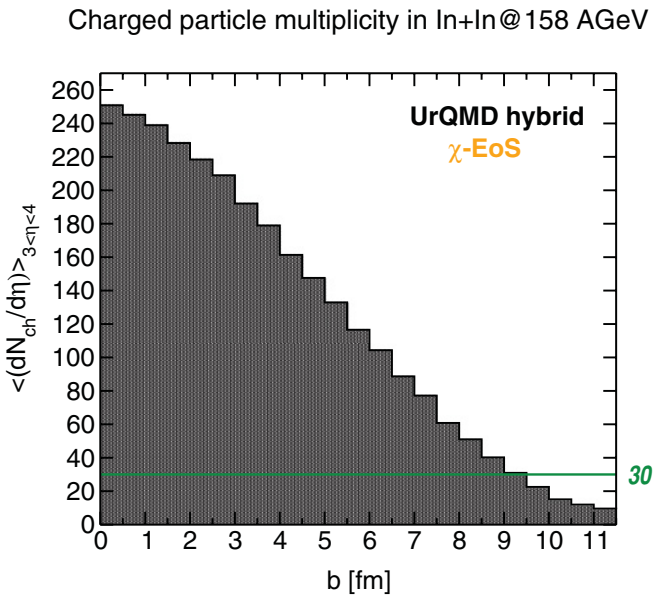

FIG. 2. (Color online) Charged particle density as a function of the impact parameter.

of the dilepton pair p_T. The theoretical spectra are normalized to the corresponding average number of charged particles in an interval of one unit of rapidity around mid-rapidity.[1] In the invariant mass region $M < 0.5$ GeV the spectra are dominated by the thermal radiation from the in-medium ρ meson. The p_T scaling exhibited compares nicely to the experimental observations.

In the region around the ρ meson peak, a net dominance of the cascade contribution is found. This result differs quite substantially from the one of previous theoretical work which adopted the sudden-freezeout approximation. It is an intrinsic feature of the hybrid model, due to the presence of a final cascade after the hydrodynamical evolution, leading to a continuous and slow decoupling of the particles. In fact, the sum of the thermal and cascade contributions leads to an overestimation of the NA60 data in the peak region for $p_T < 1$ GeV. With increasing p_T, however, the agreement with the experimental data improves. This aspect deserves further investigations and discussion but will be postponed to a separate dedicated section. If we adopt the sudden-freezeout approximation we obtain the result shown in Fig. 4. One observes that the yield in the peak region is reduced in comparison to results obtained with a full cascade-like modeling of the time scale of the freezeout process and the global result is comparable to calculations by other groups (see Fig. 4 of Ref. [3]). The component denoted with freezeout ρ and depicted by the dashed line corresponds to the dimuon yield from decays of primary ρ mesons produced at the transition.

In the intermediate-mass region, $1 < M < 1.5$ GeV, we find that emission from the QGP accounts for about half of the total radiation. The remaining half is filled by the considered hadronic sources. The 4π annihilation alone is comparable to the QGP emission only for $M > 1.4$ GeV. It is lower in the mass region $1 < M < 1.2$ GeV, where, however, the sum of the thermal and cascade ρ is not yet completely negligible. With the exception of the two lowest p_T bins, where the data are slightly underestimated in the region $1 < M < 1.2$ GeV, the description of the intermediate-mass region is reasonable. As already highlighted in the very low mass region, the p_T dependence of the thermal radiation in the intermediate-mass region is compatible with experimental observations. This latter point is noteworthy because in the three thermal approaches which have been used so far to compute dimuon spectra in comparison to NA60 data the transverse expansion is driven by two free parameters, namely the expansion velocity and the chosen radial profile (see Table 1 in Ref. [71] for the specific values and profiles used by the three groups). In the present model, on the contrary, the transverse expansion during the hydrodynamical evolution is univocally determined by the pressure of the EoS and by the initial transverse profile generated by the preceding cascade.

[1]The rapidity window covered by the NA60 detector is about one unit in the forward direction. Here, we make use of the symmetry of the system and, in order to increase statistics, we apply the specular cut $|y| < 1$ around mid-rapidity.

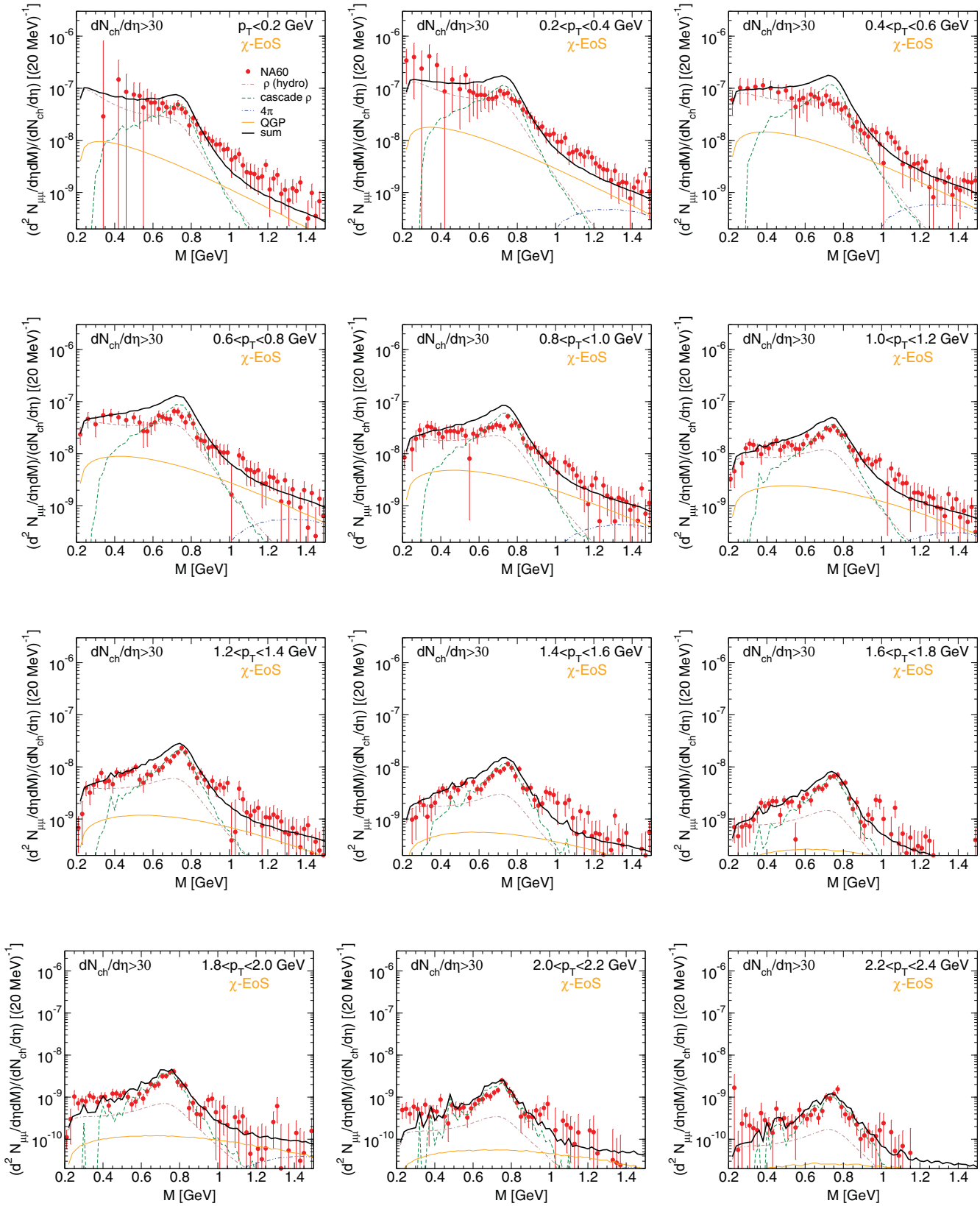

FIG. 3. (Color online) Acceptance-corrected invariant mass spectra of the excess dimuons in In-In collisions at 158A GeV for various bins of transverse pair momenta. The individual contributions arise from in-medium modified ρ mesons (dotted-dashed line), 4π annihilation (double dotted-dashed line), quark-antiquark annihilation in the QGP (thin full line), and cascade ρ mesons (dashed line). The sum of the various contributions is depicted by the thick full line. Experimental data are from Ref. [3].

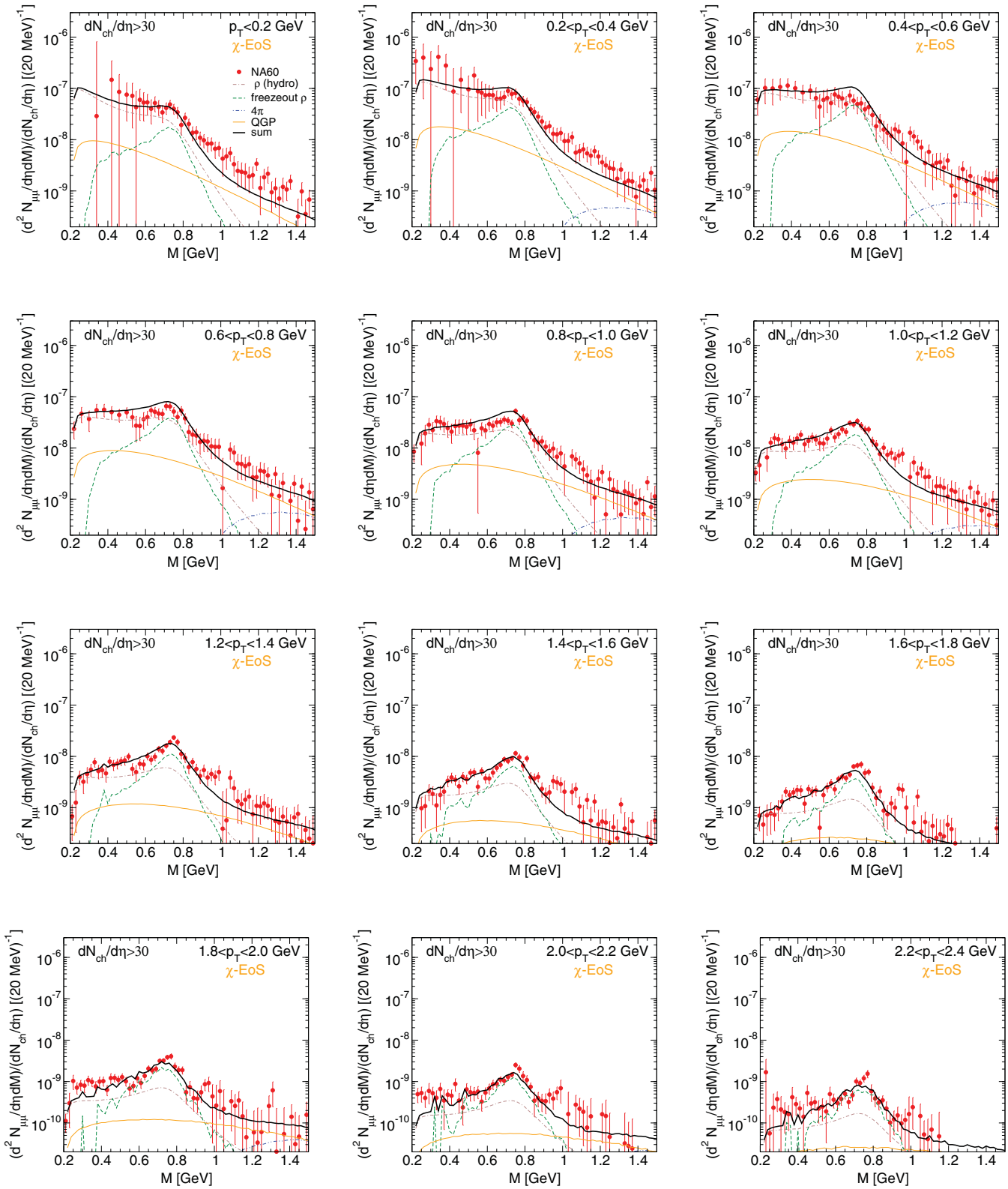

FIG. 4. (Color online) Same as Fig. 3, but with the sudden freezeout approximation.

This represents an important improvement in the field of the dynamics of thermal dileptons.

Finally, we find that the importance of the thermal contribution over the nonthermal one decreases with increasing p_T, in agreement with previous findings [9–12].

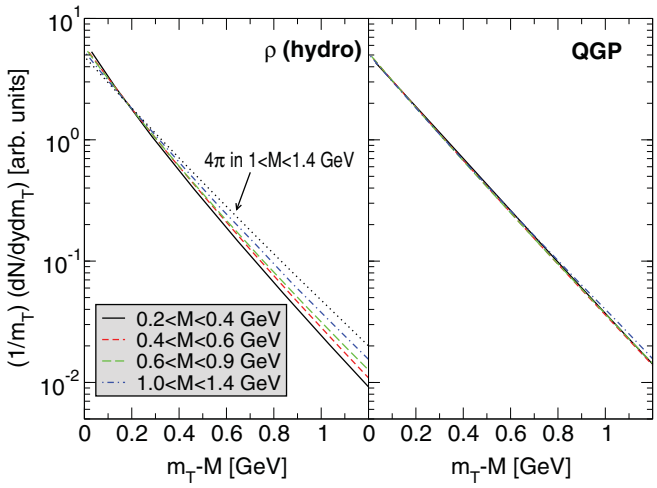

FIG. 5. (Color online) Transverse mass spectra of thermal dimuons emitted from in-medium ρ (left panel) and QGP (right panel) in four mass windows. The dotted line depicts the emission from 4π annihilation processes in the mass window $1 < M < 1.4$ GeV. The spectra are arbitrarily normalized to increase readability.

C. Transverse mass spectra

We now reverse the analysis presented in the previous section and discuss transverse mass spectra of the dimuon excess for four different bins of invariant mass. Let us first focus on the thermal emission during the hydro phase and analyze the shape of the transverse mass spectra of two sources, the emission from QGP and from a hadronic source such as the in-medium ρ. Dilepton radiation from these two contributions is shown Fig. 5. For each mass bin the corresponding transverse mass spectrum has been separately scaled by an arbitrary factor to facilitate the visualization of the differences in the slopes of the four curves. We observe that the QGP emission (right panel) presents similar slopes for all four invariant mass bins. Such an independence from the mass clearly suggests early emission from a hot low flow source. In contrast, the radiation from the in-medium ρ (left panel) exhibits a continuous hardening with increasing mass. Emission from a source with finite flow typically leads to such a mass ordering phenomenon. The same considerations explain why the 4π contribution, depicted by a dotted line in the left panel of Fig. 5, is slightly harder than the thermal ρ meson contribution in the last mass bin. Let us recall Fig. 3 and focus on the invariant mass mass region $1 < M < 1.4$ GeV: we note that the 4π contribution is more copiously localized at masses higher than the in-medium ρ.

Comparison of transverse mass spectra resulting from the present model and NA60 data is shown in Fig. 6. The model fails to describe the peculiar rise at low p_T ($m_T < 0.2$ GeV) observed experimentally. At present, no consistent physical interpretation of the rise could be achieved [3,9]. With the exception of the lowest p_T region, the model compares reasonably well with the experimental data in the lowest and highest mass bins. In the mass bin $0.4 < M < 0.6$ GeV, the overestimation of the yield observed around the peak region starts to appear, but no strong deviation in the shape of the transverse mass spectra can be observed. This is not the

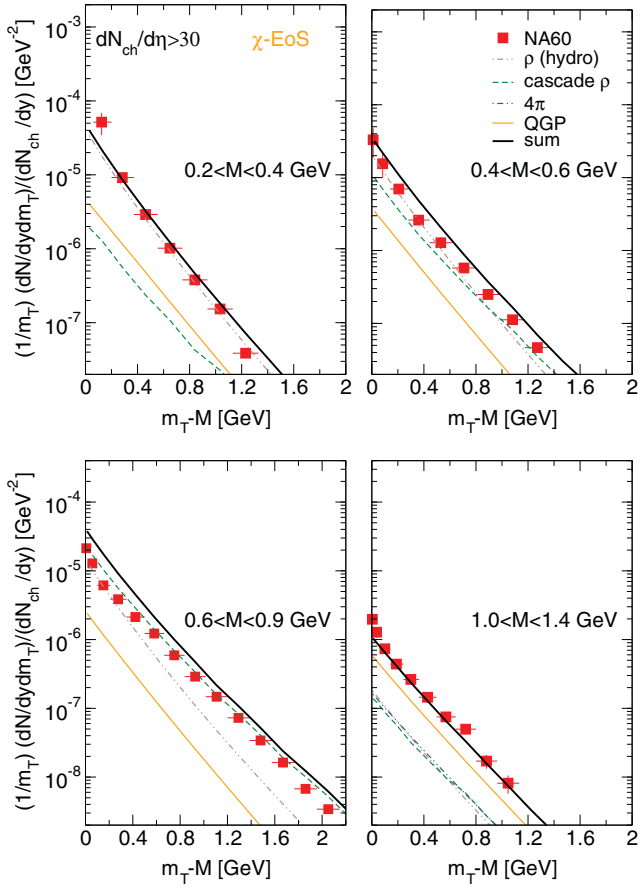

FIG. 6. (Color online) Acceptance-corrected transverse mass spectra of the excess dimuons in four mass windows. Experimental data are from Ref. [3].

case in the mass bin $0.6 < M < 0.9$ GeV, where the most severe overestimation of the yield observed at low p_T modifies substantially the resulting shape of the transverse mass spectra and clear deviations with respect to the measured spectra are observed.

Finally, the lowest mass bin is dominated by the radiation from the in-medium vector meson, whereas in the other mass bins the resulting spectra are a composition of various sources, with the exception of the high-p_T region of the $0.6 < M < 0.9$ GeV bin, where the cascade contribution clearly dominates. Turning the discussion around, we can state that the lowest mass bin can be considered as a barometer of the radiation emitted by the in-medium ρ. The reasonable agreement with the experimental observations suggests that the latter does indeed follow a dynamical path as expected from hydrodynamical models.

If we adopt the sudden-freezeout approximation we obtain the result shown in Fig. 7. This is practically identical to the previous one in the lowest and highest mass bins, whereas major differences can be observed in the two intermediate mass bins and are caused by the reduction of the nonthermal emission.

To complete our analysis of the transverse mass spectra of the dimuon excess, we follow the procedure adopted by the NA60 Collaboration and perform a quantitative

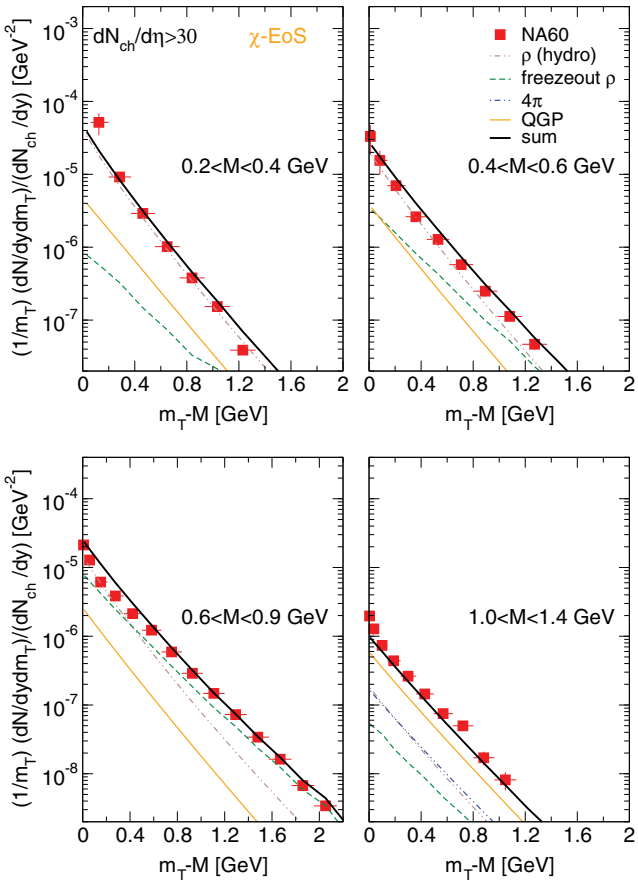

FIG. 7. (Color online) Same as Fig. 6, but with the sudden freezeout approximation.

analysis of effective slope parameters. The measured spectra have been divided into several invariant mass bins, in each of which the data have been fitted with the function $(1/m_T)dN/dm_T \propto \exp(-m_T/T_{\rm eff})$, where the effective temperature parameter $T_{\rm eff}$ is the inverse slope of the distribution. The fit range was taken as $0.4 < p_T < 1.8$ GeV, identically to the NA60 fit range [3]. We apply this procedure to the results of our calculation. The resulting exponential fits are shown in Fig. 8. In Fig. 9 the inverse slope parameters extracted from the fit procedure are plotted versus the dimuon mass, as done by the experimental collaboration. We observe that the model is able to qualitatively describe the rise of $T_{\rm eff}$ with mass up to the pole position of the ρ meson followed by a drop in the intermediate-mass region observed experimentally. However, at the quantitative level, the extracted values of $T_{\rm eff}$ reproduce the experimental ones only in the first and last mass bins, whereas they underestimate them in the second and third mass bins. One should note that a variation in the fit range, taking, e.g., the fit range chosen in Ref. [12], would increase the temperature by 8% in the first three mass bins and 3% in the latter, so that the decrease would persist. However, such a fit range would not be consistent with the experimental procedure.

At present, we can only speculate on the origin of the discrepancies in the values of the effective temperatures extracted in the mass region $0.4 < M < 0.9$ GeV. The excitation function of the mean transverse mass of various hadrons has been examined in previous works [22,35,37] where it was shown that, whereas the hybrid approach reasonably reproduces the general behavior of the mean m_T as a function of energy for various particle species, slightly higher values than the experimental data were observed for pions, protons, and negatively charged kaons produced in nucleus-nucleus collisions at the top SPS energies. Similar considerations can be drawn from the comparison of the inverse slope parameters extracted for the η, ω, and ϕ mesons by the NA60 Collaboration from the analysis of the cocktail (Fig. 9, open circles) with the respective values obtained within the present model (Fig. 9, open triangles). For completeness, the model result for the effective temperature of negatively charged pions[2] has been inserted in Fig. 9 as well. We note that the effective temperatures of the three cocktail hadrons are slightly overestimated by the hybrid approach. Thus, a more copious radial flow than the one resulting from the present model can be hardly conciliated with the overall hadron results at the same beam energy.

The model predicts for the ϕ an only slightly higher value of $T_{\rm eff}$ than for the ω, in qualitative agreement with the experimental observations, but at the same time returns comparable values for the ω and the ρ mesons, where with ρ here we intend the contribution to the total emission in the mass bin $0.6 < M < 0.9$ GeV from freezeout ρ as resulting when adopting the sudden-freezeout approximation in the calculation. In contrast, the inverse slope parameter $T_{\rm eff}$ extracted by the NA60 data for the peak region, isolated from the continuum in the mass spectrum by a side-window subtraction method and interpreted as the freezeout ρ [3], is about 50 MeV higher than that extracted for the ω mesons, of similar mass, and above the one measured for protons in Pb-Pb collisions, which are also strongly coupled to pions [72]. Such a behavior can be hardly obtained in models (such as the present one) in which decoupling from the hydrodynamical description happens simultaneously for all particle species. Nevertheless, as will be shown in the next section, a close analysis of the cascade stage that follows the hydrodynamical evolution does suggest that after the transition the ρ meson is still coupled to the medium. Within the present model, however, essentially no additional radial flow is developed in this late stage since the cascade description is characterized by softer transverse dynamics than the hydrodynamics one, so that the maximum coupling to the flow is typically reached at the end of the hydrodynamical evolution. This may suggest that the stage during which the ρ emerges from the hydrodynamical flow, with corresponding modifications of its spectral function, is too roughly described by the approximation that, instantaneously and within a layer, one may transit from an in-medium modified ρ coupled to the fluid to a vacuum-like ρ interacting according to a cascade description. Presumably, residual in-medium modifications are still present during the time span of decoupling and the cascade

[2]For the pions, the fit has been performed in the range $0 < m_T - m_0 < 0.7$ GeV; for the other hadrons, the same fit range as used for the excess, i.e., $0.4 < p_T < 1.8$ GeV, has been used.

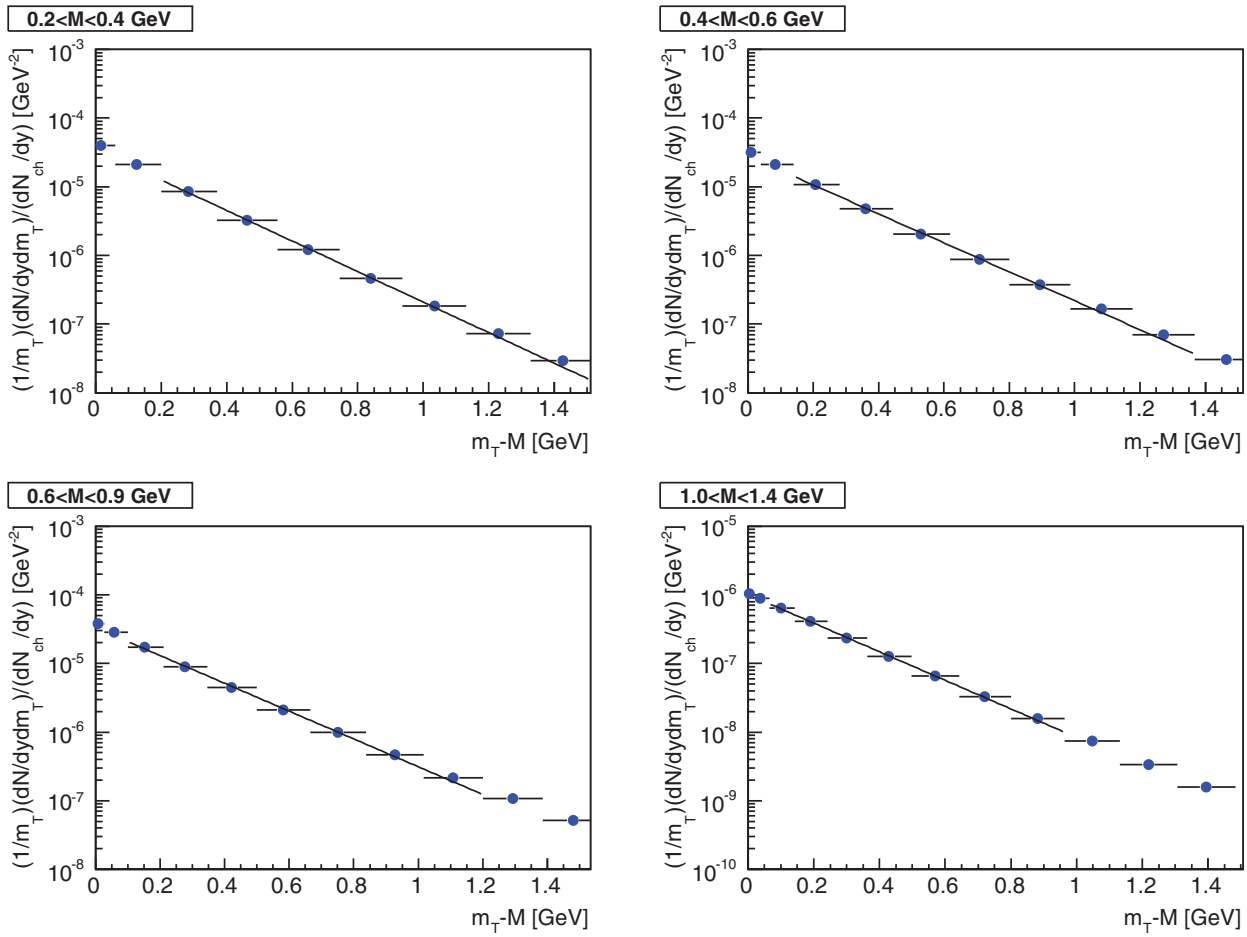

FIG. 8. (Color online) Exponential fit of the transverse mass spectra of the excess dimuons in four mass windows. The fit range is restricted to the transverse momentum interval $0.4 < p_T < 1.8$ GeV. (Note that the fit range in $m_T - M$ is different.)

stage. Escape probability arguments, as well as the analysis of the cascade stage, suggest that the ability to decouple is momentum dependent since fast particles escape earlier than slow ones. To take all these effects into account properly is not trivial and beyond of the aims of the present work. Generally such models can be constructed, as has been done, e.g., by Grassi *et al.* [73]. Indeed, indirect evidence for the presence of in-medium modifications of the low-p_T cocktail ω mesons has been observed by the NA60 Collaboration in the form of disappearance of the yield in the low-m_T region with respect to a reference exponential fit line [3]. If one assumes a similar behavior for the ρ mesons, then a depletion at low m_T of the freezeout contribution to the transverse mass spectra can be expected. Whether this can effectively result in larger values of the inverse slope parameter of the whole excess depends substantially on the relative importance of the freezeout and thermal contribution in the low-m_T region.

Another effect that may harden the transverse dynamics is the inclusion of viscosity in the hydrodynamical equations, as schematically shown in Refs. [74,75]. However, the viscous effects induce a hardening of the transverse spectra not only of dileptons but also of pions [75]; therefore a consistent interpretation of the transverse spectra of hadrons and dileptons at top SPS energy might be challenging even for viscous hydrodynamics.

IV. DECOMPOSITION OF THE CASCADE CONTRIBUTION AND DISCUSSION

In this section we want to take a closer look to the various components that enter the contribution of the cascade stage to the dimuon spectra. The total cascade emission consists of (i) the emission from the stage that precedes the hydrodynamical evolution (denoted as "pre-hydro"); (ii) the dimuon emission from the primary ρ mesons produced at the point of transition between the hydrodynamic and the cascade evolution via the Cooper-Frye equation (denoted as "Cooper"); and (iii) the emission from ρ mesons (re)generated from interactions occurring during the late cascade stage that follows the hydrodynamics evolution (denoted as "regenerated").

In Fig. 10 we show the three contributions for three different bins on transverse momentum, low (left), intermediate (center), and high (right). The emission from the stage that precedes the hydrodynamical evolution (dotted line) is negligible in comparison to the others. The contribution to

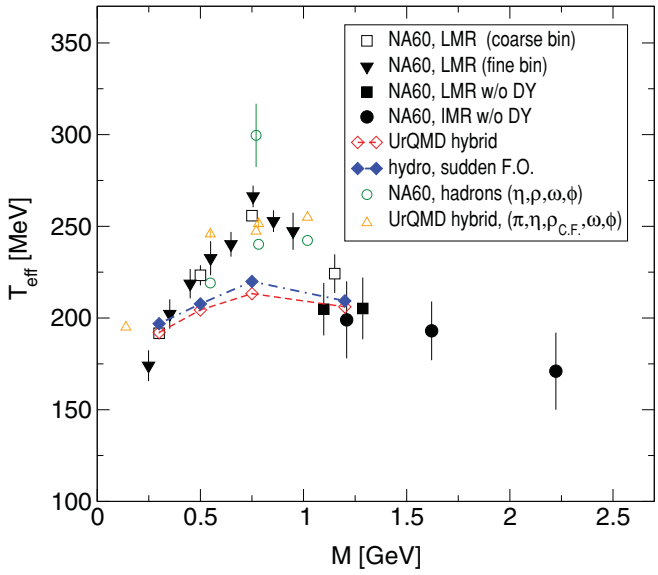

FIG. 9. (Color online) Inverse slope parameter $T_{\rm eff}$ vs dimuon invariant mass. Experimental data (full triangles, full and open squares, and full circles) are from Refs. [2,3]. The values of $T_{\rm eff}$ extracted by the fit of the calculated transverse mass spectra (shown in Fig. 6) are indicated by open diamonds. The full diamonds depict the values of $T_{\rm eff}$ extracted by the fit of the transverse mass spectra obtained using the sudden-freezeout approximation (shown in Fig. 7). The open circles depict hadron data obtained at NA60 as a by-product of the cocktail subtraction procedure (η, ω, and ϕ) and from a decomposition into peak and continuum of the ρ-like window (see Ref. [3] for details). The corresponding hybrid model results are indicated by open triangles.

dimuon emission from ρ mesons generated in the cascade stage (dotted-dashed line) is in general comparable to the one from ρ mesons created at the transition (dashed line), with its relative importance decreasing for increasing transverse momentum. This latter pattern is due to the generally more

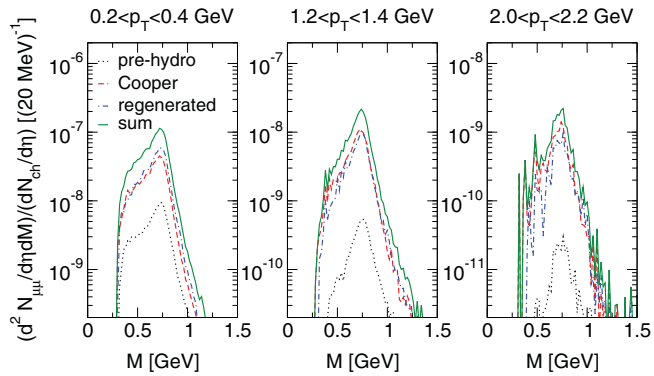

FIG. 10. (Color online) Decomposition of the cascade $\rho^0 \to \mu^+\mu^-$ emission in (i) emission from the stage that precedes the hydrodynamical evolution (dotted line); (ii) emission from ρ mesons which are merged into the cascade at the transition point via the Cooper- Frye equation and emit in the cascade stage of the evolution (dashed line); and (iii) emission from ρ mesons which are produced and emit in the cascade stage (dotted-dashed line). The full line represents the total cascade emission.

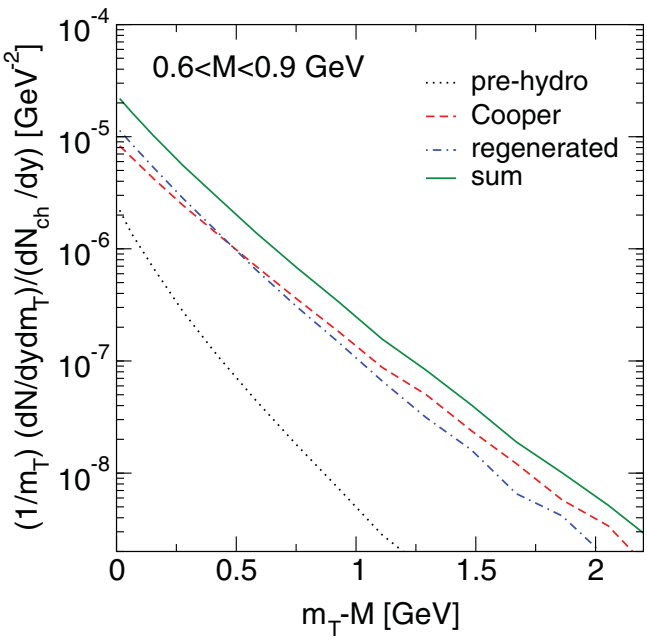

FIG. 11. (Color online) Decomposition of the cascade $\rho^0 \to \mu^+\mu^-$ emission as in Fig. 10, but for transverse mass spectra.

moderate transverse dynamics of cascade approaches in comparison to hydrodynamical models, as pointed out by various studies on transverse mass spectra of different hadron species performed within the present framework [23,36,37] and by a previous independent comparative analysis of hadronic cascade dynamics versus hydrodynamics done by Huovinen *et al.* [76]. A more explicit view of the effect is shown in Fig. 11 where the transverse mass spectra of the three components are presented separately. We see that the contribution to dimuon emission from ρ mesons that are merged into the cascade at the transition point via the Cooper-Frye equation and emit in the cascade stage of the evolution (dashed line) has flatter spectra than the one from ρ mesons generated in the cascade stage (dotted-dashed line). The emission from the stage that precedes the hydrodynamical evolution presents as well steeper spectra than the one from ρ mesons generated at the transition point (the latter being maximally coupled to the flow). The reason is that this contribution is mainly due to early decay of ρ mesons generated by string excitation in first chance nucleon-nucleon collisions and therefore resembles closely the steep trend exhibited by dimuon transverse spectra in pp collisions.

Returning to the comparison with NA60 data shown in Fig. 3, we found that the sum of the thermal and the cascade contributions lead to an overestimation of the peak region. The reason for the disagreement might be twofold:

(i) As mentioned in the previous section, it can be argued that in-medium modifications of the spectral shape of the ρ meson are still important during the cascade stage and cannot be neglected as typically done in cascade models. The authors of Ref. [12], e.g., took partially into account in-medium modifications of the freezeout contribution by employing, at freezeout, the vacuum form of the ρ self-energy augmented with a width

corresponding to the full width at half-maximum of the in-medium spectral function at the freezeout conditions. This procedure allows one to effectively account for resonance decays figuring into the ρ self-energy with the net effect of depleting the yield in the peak region. In contrast, if resonance decays are simply added channel by channel in a perturbative way, the net effect is the opposite, i.e., to enhance the yield in the peak region. (This property is quite general; see, e.g., the discussion in Refs. [63,70].) It might be interesting to investigate these two scenarios more in detail in the future.

(ii) It can be as well argued that the modeling of the freezeout time scale via hadronic cascade delivers a too slow decoupling of the ρ meson as a consequence of a longer persistence of the "pion wind" via processes such as, e.g., $\pi\pi \to \rho \to \pi\pi$ and $\pi N \to N^*/\Delta^* \to \rho N$. Concerning this point, independent information might be obtained from Hanbury-Brown-Twiss interferometry (HBT) analyses. The analysis of HBT radii of pions produced in heavy-ion collisions at the SPS energy regime performed within the hybrid approach used in this work indeed suggested that at top SPS energy a shorter duration time of the freezeout process than the one obtained from the inclusion of a cascade stage after the hydrodynamical evolution may be favored by experimental data [77]. An HBT analysis of dilepton emission might help to shed some light on the decoupling time of the ρ meson and presumably reveal interesting features of the space extension of the sources contributing to the various invariant mass regions.

V. SUMMARY AND CONCLUSIONS

In this work we employed an integrated Boltzmann + hydrodynamics hybrid approach based on the ultrarelativistic quantum molecular dynamics transport model with an intermediate (3 + 1)-dimensional hydrodynamic stage to analyze the hadronic contribution to the dimuon excess observed in In + In collisions at $E_{\rm lab} = 158A$ GeV. We found that three regions can be identified in the dilepton invariant spectra. The very low mass region of the spectrum is dominated by thermal radiation, the region around the ρ meson peak is dominated by late stage cascade dilepton emission, and the intermediate region receives contributions from both hadronic and QGP emission, with the QGP accounting for about half of the total emission. The invariant mass regions $M < 0.5$ GeV and $M > 1$, dominated by thermal radiation, show reasonable p_T scaling, revealing that if thermal rates are convoluted in a dynamical model a comprehensive interpretation of the M and p_T path observed experimentally can be achieved. The model, however, fails in describing the region around the vector meson peak for low p_T, mostly due to the presence of a copious emission during the cascade which follows the hydrodynamical evolution. The comparison to experimental data seems to disfavor the presence of a long-lived cascade emission in which the ρ meson can be approximated by its vacuum properties.

The present calculation represents a first effort toward a more consistent treatment of the dynamics of thermal dileptons from in-medium modified hadrons as well as nonhadronic sources, which was so far entrusted to more schematic models. In this paper, we discussed the dimuon invariant mass region $2m_\mu < M < 1.5$ GeV. The NA60 experiment, however, has succeeded in isolating the excess also in the region $1.5 < M < 2.6$ GeV [48], and a nice matching between the low- and the intermediate-mass-region analyses was achieved [48,78]. Extension of the present approach in order to enable the investigation of invariant masses up to 2.6 GeV is highly desirable and planned for the future. We expect it to bring further insights into the role of partonic contributions to the dimuon excess measured in the intermediate-mass region.

ACKNOWLEDGMENTS

The authors acknowledge useful discussions with R. Rapp, H. van Hees, and B. Bäuchle. G. Moschelli and T. Kolleger are thanked for their assistance in the use of ROOT. We thank S. Damjanovic for providing the experimental data. This work was supported by the Hessen Initiative for Excellence (LOEWE) through the Helmholtz International Center for FAIR (HIC for FAIR). Computational resources have been provided by the Center for Scientific Computing.

[1] R. Arnaldi *et al.* (NA60 Collaboration), Phys. Rev. Lett. **96**, 162302 (2006).
[2] R. Arnaldi *et al.* (NA60 Collaboration), Phys. Rev. Lett. **100**, 022302 (2008).
[3] R. Arnaldi *et al.* (NA60 Collaboration), Eur. Phys. J. C **61**, 711 (2009).
[4] R. Arnaldi *et al.* (NA60 Collaboration), Phys. Rev. Lett. **102**, 222301 (2009).
[5] G. Agakichiev *et al.* (CERES Collaboration), Phys. Rev. Lett. **75**, 1272 (1995).
[6] M. A. Mazzoni (HELIOS/3 Collaboration), Nucl. Phys. A **566**, 95c (1994).
[7] H. van Hees and R. Rapp, Phys. Rev. Lett. **97**, 102301 (2006).
[8] K. Dusling, D. Teaney, and I. Zahed, Phys. Rev. C **75**, 024908 (2007).
[9] T. Renk and J. Ruppert, Phys. Rev. C **77**, 024907 (2008).
[10] K. Dusling and I. Zahed, Phys. Rev. C **80**, 014902 (2009).
[11] J. Ruppert, C. Gale, T. Renk, P. Lichard, and J. I. Kapusta, Phys. Rev. Lett. **100**, 162301 (2008).
[12] H. van Hees and R. Rapp, Nucl. Phys. A **806**, 339 (2008).
[13] P. Huovinen, P. V. Ruuskanen, and J. Sollfrank, Nucl. Phys. A **650**, 227 (1999).
[14] P. Huovinen and M. Prakash, Phys. Lett. B **450**, 15 (1999).
[15] P. Huovinen, M. Belkacem, P. J. Ellis, and J. I. Kapusta, Phys. Rev. C **66**, 014903 (2002).
[16] P. Huovinen, P. V. Ruuskanen, and S. S. Rasanen, Phys. Lett. B **535**, 109 (2002).
[17] M. M. Aggarwal *et al.* (WA98 Collaboration), Phys. Rev. Lett. **85**, 3595 (2000).
[18] A. Dumitru, S. A. Bass, M. Bleicher, H. Stoecker, and W. Greiner, Phys. Lett. B **460**, 411 (1999).
[19] S. A. Bass *et al.*, Phys. Rev. C **60**, 021902 (1999).

[20] T. Hirano, U. W. Heinz, D. Kharzeev, R. Lacey, and Y. Nara, Phys. Lett. B **636**, 299 (2006).
[21] B. Bauchle and M. Bleicher, Phys. Rev. C **81**, 044904 (2010).
[22] H. Petersen, J. Steinheimer, G. Burau, M. Bleicher, and H. Stocker, Phys. Rev. C **78**, 044901 (2008).
[23] E. Santini, H. Petersen, and M. Bleicher, Phys. Lett. B **687**, 320 (2010).
[24] B. Bauchle and M. Bleicher, Phys. Rev. C **82**, 064901 (2010).
[25] B. Bauchle and M. Bleicher, Phys. Lett. B **695**, 489 (2011).
[26] E. Santini and M. Bleicher, J. Phys. Conf. Ser. **270**, 012040 (2011).
[27] S. A. Bass *et al.*, Prog. Part. Nucl. Phys. **41**, 255 (1998).
[28] M. Bleicher *et al.*, J. Phys. G **25**, 1859 (1999).
[29] H. Petersen, M. Bleicher, S. A. Bass, and H. Stocker, arXiv:0805.0567 [hep-ph].
[30] J. Steinheimer *et al.*, Phys. Rev. C **77**, 034901 (2008).
[31] H. Petersen and M. Bleicher, Phys. Rev. C **79**, 054904 (2009).
[32] D. H. Rischke, S. Bernard, and J. A. Maruhn, Nucl. Phys. A **595**, 346 (1995).
[33] D. H. Rischke, Y. Pursun, and J. A. Maruhn, Nucl. Phys. A **595**, 383 (1995).
[34] H. Petersen, J. Steinheimer, G. Burau, and M. Bleicher, Nucl. Phys. A **830**, 283c (2009).
[35] J. Steinheimer, V. Dexheimer, H. Petersen, M. Bleicher, S. Schramm, and H. Stocker, Phys. Rev. C **81**, 044913 (2010).
[36] Q.-F. Li, J. Steinheimer, H. Petersen, M. Bleicher, and H. Stocker, Phys. Lett. B **674**, 111 (2009).
[37] H. Petersen, J. Steinheimer, M. Bleicher, and H. Stocker, J. Phys. G **36**, 055104 (2009).
[38] H. Petersen, J. Steinheimer, G. Burau, and M. Bleicher, Eur. Phys. J. C **62**, 31 (2009).
[39] F. Cooper and G. Frye, Phys. Rev. D **10**, 186 (1974).
[40] J. Steinheimer, S. Schramm, and H. Stocker, J. Phys. G **38**, 035001 (2011).
[41] P. Papazoglou, S. Schramm, J. Schaffner-Bielich, H. Stocker, and W. Greiner, Phys. Rev. C **57**, 2576 (1998).
[42] P. Papazoglou *et al.*, Phys. Rev. C **59**, 411 (1999).
[43] V. Dexheimer and S. Schramm, Astrophys. J. **683**, 943 (2008).
[44] K. Fukushima, Phys. Lett. B **591**, 277 (2004).
[45] C. Gale and J. I. Kapusta, Nucl. Phys. B **357**, 65 (1991).
[46] R. Rapp and J. Wambach, Adv. Nucl. Phys. **25**, 1 (2000).
[47] V. L. Eletsky, M. Belkacem, P. J. Ellis, and J. I. Kapusta, Phys. Rev. C **64**, 035202 (2001).
[48] R. Arnaldi *et al.* (NA60 Collaboration), Eur. Phys. J. C **59**, 607 (2009).
[49] Z. Huang, Phys. Lett. B **361**, 131 (1995).
[50] C. Song, C. M. Ko, and C. Gale, Phys. Rev. D **50**, 1827 (1994).
[51] P. Lichard and J. Juran, Phys. Rev. D **76**, 094030 (2007).
[52] B. Aubert *et al.* (BABAR Collaboration), Phys. Rev. D **71**, 052001 (2005).
[53] M. N. Achasov *et al.*, J. Exp. Theor. Phys. **96**, 789 (2003).
[54] R. R. Akhmetshin *et al.* (CMD-2 Collaboration), Phys. Lett. B **475**, 190 (2000).
[55] R. R. Akhmetshin *et al.* (CMD-2 Collaboration), Phys. Lett. B **595**, 101 (2004).
[56] D. Bisello *et al.* (DM2 Collaboration), Nucl. Phys. Proc. Suppl. **21**, 111 (1991).
[57] V. P. Druzhinin, arXiv:0710.3455 [hep-ex].
[58] J. Cleymans, J. Fingberg, and K. Redlich, Phys. Rev. D **35**, 2153 (1987).
[59] K. Schmidt *et al.*, Phys. Rev. C **79**, 064908 (2009).
[60] G.-Q. Li and C. M. Ko, Nucl. Phys. A **582**, 731 (1995).
[61] S. Vogel *et al.*, Phys. Rev. C **78**, 044909 (2008).
[62] E. L. Bratkovskaya and W. Cassing, Nucl. Phys. A **807**, 214 (2008).
[63] J. Knoll, Prog. Part. Nucl. Phys. **42**, 177 (1999).
[64] S. Leupold, Nucl. Phys. A **672**, 475 (2000).
[65] Y. B. Ivanov, J. Knoll, and D. N. Voskresensky, Nucl. Phys. A **672**, 313 (2000).
[66] W. Cassing and S. Juchem, Nucl. Phys. A **677**, 445 (2000).
[67] J. Knoll, Y. B. Ivanov, and D. N. Voskresensky, Ann. Phys. **293**, 126 (2001).
[68] S. Juchem, W. Cassing, and C. Greiner, Phys. Rev. D **69**, 025006 (2004).
[69] S. Juchem, W. Cassing, and C. Greiner, Nucl. Phys. A **743**, 92 (2004).
[70] B. Friman, C. Höhne, J. Knoll, S. Leupold, J. Randrup, R. Rapp, and P. Senger, eds., *The CBM Physics Book: Compressed Baryonic Matter in Laboratory Experiments*, Lecture Notes in Physics, Vol. 814 (Springer, New York, 2011).
[71] R. Rapp, J. Wambach, and H. van Hees, in *Relativistic Heavy Ion Physics*, Landolt-Börnstein: Numerical Data and Functional Relationships in Science and Technology—New Series, edited by R. Stock (Springer, New York, 2010).
[72] R. Arnaldi *et al.* (NA60 Collaboration), J. Phys. G **37**, 094030 (2010).
[73] F. Grassi, Y. Hama, and T. Kodama, Phys. Lett. B **355**, 9 (1995).
[74] K. Dusling and S. Lin, Nucl. Phys. A **809**, 246 (2008).
[75] T. Song, K. C. Han, and C. M. Ko, Phys. Rev. C **83**, 024904 (2011).
[76] P. Huovinen, P. Kolb, U. W. Heinz, P. Ruuskanen, and S. Voloshin, Phys. Lett. B **503**, 58 (2001).
[77] C. Alt *et al.* (NA49 Collaboration), Phys. Rev. C **77**, 064908 (2008).
[78] S. Damjanovic, R. Shahoyan, and H. J. Specht (NA60 Collaboration), CERN Cour. **49N9**, 31 (2009).